

Communication

Polarization Selective Broad/Triple Band Absorber Based on All-Dielectric Metamaterials in Long Infrared Regime

Haotian Zou ¹ , Bo Ni ^{2,*}, Hua Zhou ², Haibin Ni ², Guohuan Hua ² and Jianhua Chang ²

¹ Changwang School of Honors, Nanjing University of Information Science and Technology, Nanjing 210044, China; htzou328@163.com

² Jiangsu Key Laboratory of Meteorological Observation and Information Processing, School of Electronic and Information Engineering, Nanjing University of Information Science and Technology, Nanjing 210044, China

* Correspondence: bni@nuist.edu.cn

Abstract: In this paper, a polarization selective broad/triple-band metamaterial absorber based on SiO₂ all-dielectric is designed and studied. The absorber works in a long infrared band (8–14 μm). It is composed of cuboid and trapezoidal silica structures in the upper layer and metal plates in the lower layer. We calculate the absorption results of the metamaterial absorber at different polarization angles as the polarization angle of incident light increases from 0° to 90°; that is, the light changes from Ex polarization to Ey polarization. The results show that the absorption rate of the structure is more than 90% in the range of 8.16 to 9.61 μm when the polarization angle is 0°. When the polarization angle of the incident light is less than 45°, the absorption result of the absorber does not change significantly. When the polarization angle of the incident light is greater than 45°, three absorption peaks appear in the long infrared band, realizing the selectivity of the polarization of the incident light. When the polarization angle increases to 90°, the absorptivity of the two absorption peaks at λ = 9.7 μm and 12.3 μm reaches more than 85%. In addition, the sensitivity analysis of the length, width, and thickness of the all-dielectric metamaterial absorber and the calculation of the electric field of this structure are also carried out. The designed all-dielectric metamaterial absorber has polarization selection and perfect absorption characteristics and has a broad application prospect.

Keywords: polarization selective; absorber; all-dielectric metamaterials; long infrared regime



Citation: Zou, H.; Ni, B.; Zhou, H.; Ni, H.; Hua, G.; Chang, J.

Polarization Selective Broad/Triple Band Absorber Based on All-Dielectric Metamaterials in Long Infrared Regime. *Photonics* **2023**, *10*, 587. <https://doi.org/10.3390/photronics10050587>

Received: 17 April 2023

Revised: 13 May 2023

Accepted: 17 May 2023

Published: 18 May 2023



Copyright: © 2023 by the authors. Licensee MDPI, Basel, Switzerland. This article is an open access article distributed under the terms and conditions of the Creative Commons Attribution (CC BY) license (<https://creativecommons.org/licenses/by/4.0/>).

1. Introduction

A metamaterial is a kind of structural material composed of artificially designed sub-wavelength structural elements arranged periodically. It has some unusual electromagnetic properties that natural materials do not have, such as a negative refractive index [1,2], electromagnetic stealth [3], and a superlens effect [4,5]. The wavelength, phase, polarization state, angular momentum, and propagation direction of electromagnetic waves can be flexibly and effectively controlled by metamaterials. A metamaterial absorber is a kind of artificial device that can adjust electromagnetic parameters by shape, structure, and size, and then achieve a high absorption rate of electromagnetic waves in a specific frequency range [6–8]. It has the advantages of wide bandwidth, polarization selection, versatility, and so on. It has good applications and great prospects in stealth technology, polarization deflection, thermal imaging, perfect lenses, and other fields [9–11]. The concept of a perfect absorber was first proposed by Landy et al. in 2008 [6]. From the point of view of the absorption effect, perfect absorbers can be divided into narrowband [6], broadband [12], dual-band [13], multi-band [14,15] perfect absorbers, and polarization-insensitive [16] perfect absorbers. At present, most tunable metamaterial absorbers are based on graphene and alum. The tunable metamaterial absorber is designed by exploiting the sensitivity of graphene to external electric fields. The electromagnetic parameters of the metamaterial absorber are tuned by applying different voltages to graphene to change the Fermi level of graphene. The different states of alum before and after the phase transition, especially

the metal state after the phase transition, were used to realize the tuning characteristics of the metamaterial absorber. Tunable metamaterial absorbers, which can adjust the performance of metamaterial absorbers by changing the external field, have received much attention [17–19]. In addition to changing the external field, the electromagnetic characteristics of the metamaterial absorber can be adjusted by changing the polarization direction of the incident electromagnetic wave, so that the metamaterial absorber can absorb the incident electromagnetic wave in different frequency ranges at different polarization directions and then achieve the selective absorption of the incident wave in a specific polarization direction, showing the polarization selective absorption phenomenon. Polarization selective absorption plays an important role in communication [20–22], radar [23], imaging systems [5,24], etc.

At present, most metamaterial absorbers contain metal materials [25], and the design structure of such metamaterial absorbers is mostly a sandwich structure. The upper layer of the structure is a subwavelength metal structure designed manually, the middle is a dielectric layer, and the bottom is a metal layer. H. Tao [26] et al. used a metal ring resonant structure, a dielectric layer, and a metal film to achieve a narrowband perfect absorption rate of up to 97% at 1.6 THz. In 2018, Li et al. designed a dual-band absorber [27], which uses composite layers composed of germanium and gold to form a trapezoidal structure, and the structure achieves more than 80% absorption at 4~6.3 μm . The design idea of such metal structures is widely used [28,29]. However, metamaterial absorbers containing metal structures are difficult to use in large areas due to their narrow bandwidth, high ohmic loss, low melting point, difficulty in preparation, and high price. The use of dielectric materials to design the structure of the all-dielectric metamaterial absorber can minimize the loss of the dielectric material to the incident electromagnetic wave. With the gradually mature medium manufacturing process and relatively low price, the all-dielectric metamaterial absorber has received widespread attention [30–33]. In 2020, Si [34] et al. designed a broadband perfect absorber based on all-dielectric silicon, which achieved more than 95% perfect absorption between 564 nm and 584 nm, and more than 85% absorption results can also be obtained through experimental fabrication. Compared with metal absorbers, all-dielectric metamaterials are easier to broaden the absorption bandwidth and are more resistant to high temperatures [35–37], so they have broad application prospects.

In this paper, an all-dielectric polarization selective metamaterial absorber based on silicon dioxide is designed to achieve perfect absorption of the incident wave in a specific broadband. The absorption results of the metamaterial absorber at different polarization angles are calculated when the polarization angle of incident light increases from 0° to 90° ; that is, the light changes from E_x polarization to E_y polarization. The calculated results show that the absorption rate of the structure is more than 90% between 8.16 μm and 9.61 μm when the polarization angle is 0° . At the resonance wavelength $\lambda = 8.5 \mu\text{m}$, the highest absorption rate reaches 99.5%. In addition, the structure has strong polarization angle selectivity of the incident light. When the polarization angle of the incident light is less than 45° , the absorption result of the absorber does not change significantly. When the polarization angle of the incident light is greater than 45° , three absorption peaks appear in the long infrared band. When the polarization angle is increased to 90° , the absorption rates of the two absorption peaks at $\lambda = 9.7 \mu\text{m}$ and $\lambda = 12.3 \mu\text{m}$ both reach more than 85%. The proposed all-dielectric metamaterial absorber works in a long infrared regime and can achieve almost perfect absorption in a specific wavelength range, which can be used to manufacture infrared stealth materials [9]. All-dielectric polarization-selective absorbers can be used to selectively absorb light in the polarization direction in infrared optical imaging to obtain clearer and high-resolution images. It is widely used in practical imaging equipment such as thermal imagers and infrared cameras [38]. In addition, this research can also be applied to optical communication [39], optical sensors, solar cells, and other fields, providing new possibilities for research in these fields.

2. Design of Broadband Absorber Based on All-Dielectric

The structure of the all-dielectric metamaterial absorber is shown in Figure 1. We combined the trapezoidal SiO₂ structure with the cuboid SiO₂ structure and placed them on the bottom metal plate to form a structural unit. The bottom length of the trapezoidal SiO₂ structure l_2 is 1 μm , the top length l_3 is 0.6 μm , and the height h_2 is 1.3 μm . The length of the upper and lower sides of the cuboid arranged on the left side l_4 is 0.6 μm , the height of the cuboid h_1 is 2.5 μm , and the length of the two SiO₂ structures is 2 μm . Both structures were placed on a metal plate with a period l_1 of 1.6 μm , and the thickness of the metal plate was 100 nm, which can completely prevent light from penetrating through the absorber. The permittivity of SiO₂ and Au in the structural calculation were selected from Palik's work [40].

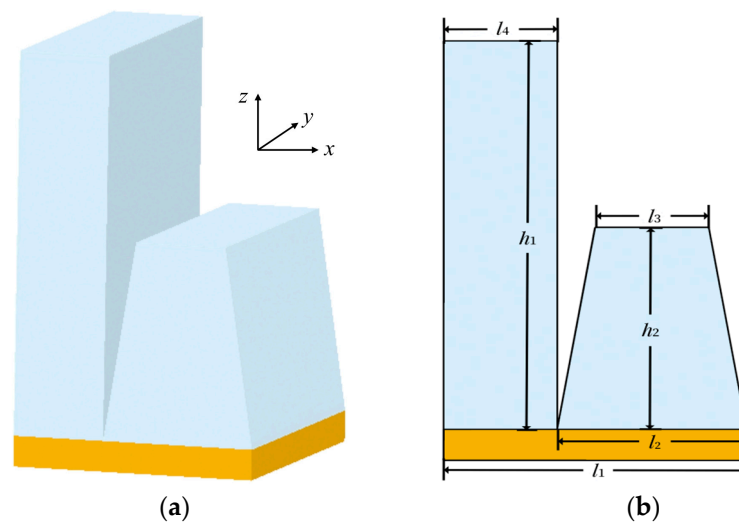


Figure 1. (a) Broadband absorber structure based on SiO₂, (b) side view.

3. Results and Discussion

3.1. Results of Broadband Absorber

The electromagnetic wave absorption rates of the two components of the above broadband absorber structure are calculated under the condition that the polarization direction of the incident light is along the Ex direction and the normal incident direction, and the calculation results are shown in Figure 2. The black solid line represents the absorption result of a single trapezoidal structure absorber, and the black dotted line represents the absorption result of a single rectangular structure absorber. It can be seen that in the band of 7–11 μm , these two structures have certain absorption phenomena. The bandwidth of the trapezoidal structure is narrow and approximately between 9 and 10 μm . The absorption rate of the absorption line of the rectangular structure is low and tends to be in the range of 8–9 μm . The combination of these two absorber structures can superpose these two continuous peaks to form a relatively complete broadband absorption peak, as shown in Figure 2, with the red solid line. The width of more than 90% absorption rate (8.16–9.61 μm) is about 1.45 μm . At the resonance wavelength $\lambda = 8.5 \mu\text{m}$, the maximum absorption rate is more than 99.5%, which has a good absorption performance. The FWHM of the structure is 2.26 μm .

In order to better study the electromagnetic wave absorption mechanism of the broadband absorber, we have carried out the electric field calculation of this structure at the polarization angle of the incident light of 0°, as shown in Figure 3:

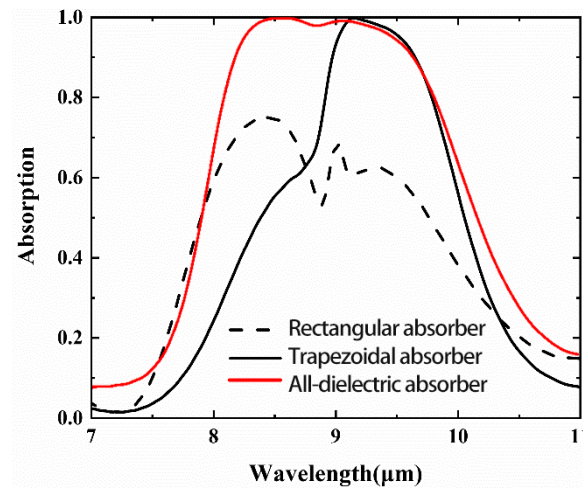


Figure 2. Absorption curves of partial structure and overall structure.

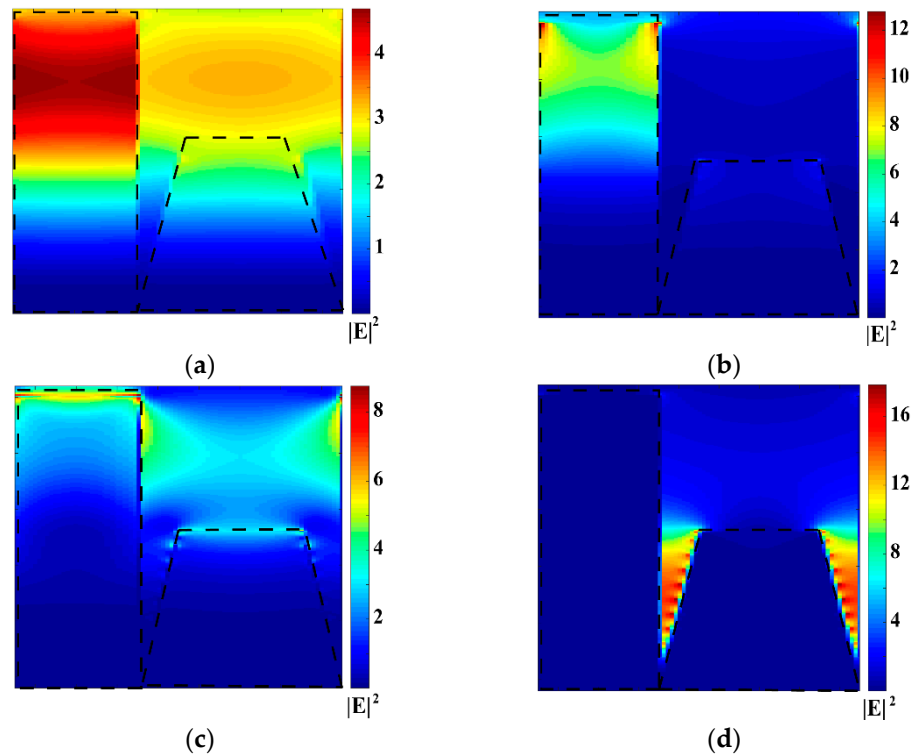


Figure 3. Electric fields at different operating wavelengths. (a) The electric field at a wavelength of 7.5 μm ; (b) an electric field at a wavelength of 8 μm ; (c) an electric field at a wavelength of 8.6 μm ; (d) the electric field at the wavelength of 9.7 μm .

The electric field E distributions at 7.5 μm , 8 μm , 8.6 μm , and 9.7 μm bands were selected for analysis. Figure 3a shows the electric field distribution at a wavelength of 7.5 μm . Compared with the electric field distribution at a wavelength of 9.7 μm in Figure 3d, the electric field intensity is only half, and the absorption rate is increased from 16% at 7.5 μm to 86% at 9.7 μm . As can be seen from the electric field distribution in Figure 3b, the electric field at the wavelength of 8 μm is mainly distributed inside the top of the rectangular absorber. As can be seen from the electric field distribution in Figure 3c, when the wavelength is redshifted to 8.6 μm , the electric field intensity inside the rectangular absorber decreases, and the electric field appears on the top of the trapezoidal absorber. At the same time, the coupling between the rectangular absorber and the trapezoidal absorber occurs, so that the absorption rate reaches the highest value of 99.5%. When the wavelength

is redshifted to 9.7 μm , as shown in Figure 3d, the electric field is mainly distributed on both sides of the trapezoidal absorber, and there is no electric field distribution on the top of the rectangular absorber, so the absorption rate drops to 86%.

3.2. Polarization Direction Analysis of Incident Light in Perfect Absorber

Figure 4 shows the comparison of absorption spectra under different polarized light vertical incidences. When the polarization angle of light increases from 0° to 90° , that is, the light changes from E_x polarization to E_y polarization, we can see that with the increasing polarization angle, three modes of absorption peaks appear in the band of 6~15 μm : The corresponding bands of λ_1 , λ_2 , and λ_3 are 8.5 μm , 9.7 μm , and 12.3 μm , respectively. In the band of 6~15 μm , the absorption peak has a certain redshift with the increase in the polarization angle. At the same time, the wide absorption peak between 8 μm and 10 μm is divided into two absorption peaks λ_1 and λ_2 with narrow FWHM due to the interference effect caused by light excitation at different wavelengths in the medium. When the polarization angle of the incident light is greater than 45° , a gradually enhanced absorption peak (mode λ_3) appears in the near ultra-far infrared band.

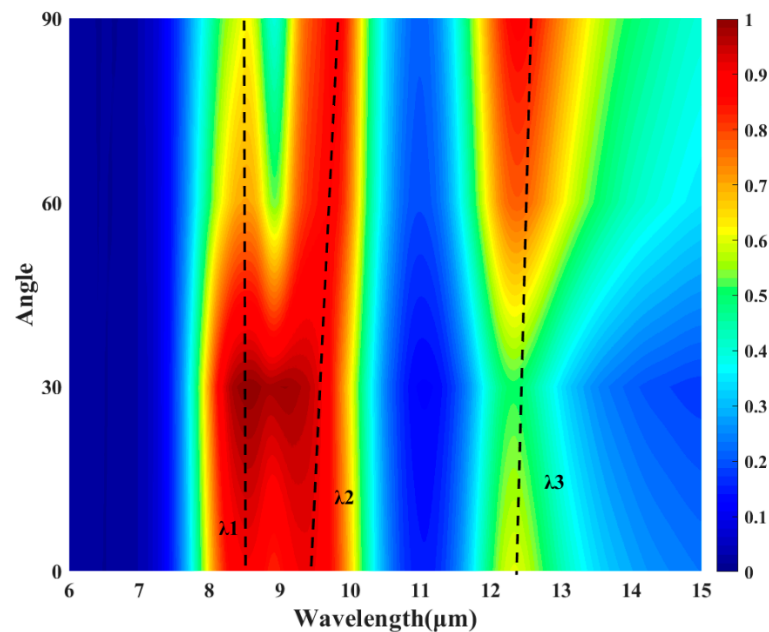


Figure 4. Spectrograms at different polarization angles.

It can be seen from Figure 4 that the absorption spectrum of the all-dielectric metamaterial absorber approximately takes the polarization angle of 45° as the selection dividing line. When the polarization angle of the incident light is less than 45° , the absorption results of the absorber do not change significantly. When the polarization angle of the incident light is greater than 45° , three absorption peaks appear in the long infrared band. When the polarization angle is increased to 90° , the absorption rates of the two absorption peaks at $\lambda = 9.7 \mu\text{m}$ and $\lambda = 12.3 \mu\text{m}$ both reach more than 85%, as shown in Figure 5.

3.3. Comparison of Different Parameters of Broadband Absorber

In the actual production, due to technical reasons, the actual value of the produced structure is generally different from the theoretical value. In order to consider the influence of various parameters on the final result, we carry out the sensitivity analysis of various parameters of the broadband absorber when the polarization angle of the incident light is 0° and 90° , including: the top of the trapezoid l_3 , the bottom of the trapezoid l_2 , the width of the rectangle l_4 , the height of the trapezoid h_2 , and the height of the rectangle h_1 .

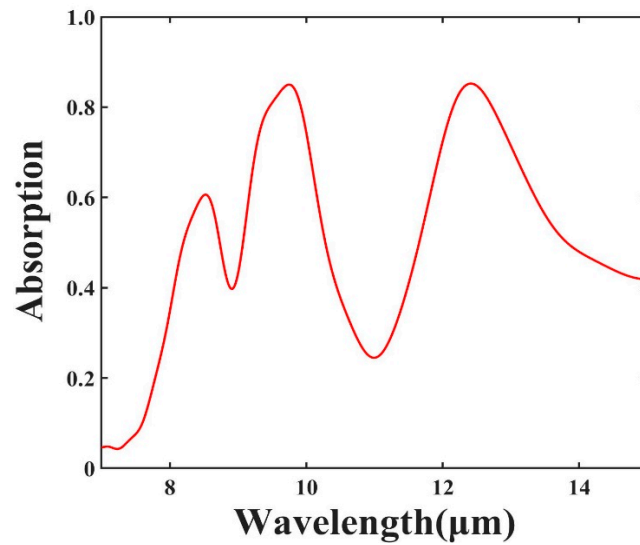


Figure 5. Absorption curves at an incidence angle of 90°.

Figure 6 shows the influence of changing the lower side length l_2 of the trapezoid in the absorber structure on the absorption results when the other parameter conditions are unchanged. Figure 6a,b, respectively, show the changing absorption curves of the incident light with different l_2 lengths under Ex polarization and Ey polarization. In Figure 6a, it can be seen that when the polarization angle of the incident light is 0°, the width of the absorption peak is slightly reduced and the absorption rate is gradually increased with the gradual increase of l_2 length. When the length of l_2 is 0.6 μm, a small wave valley appears at the wavelength of 9 μm. The overall absorption rate of the absorber can maintain above 80% during the change of l_2 . In Figure 6b, it can be seen that when the polarization angle of the incident light is 90°, the absorption of the first two absorption peaks does not change significantly with the increase in the length of l_2 . The absorption peak at $\lambda = 12.3 \mu\text{m}$ gradually decreases, and the overall absorption frequency does not change.

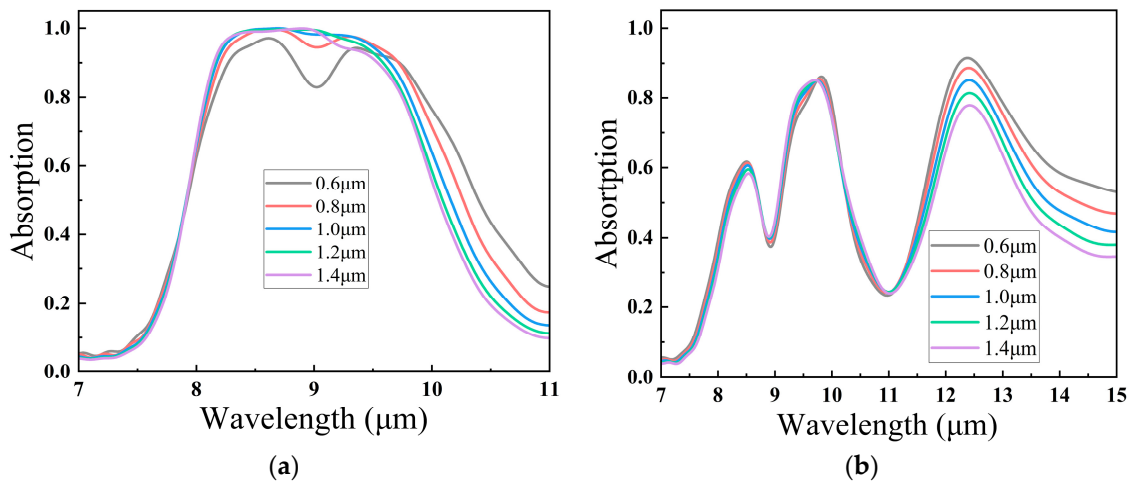


Figure 6. (a) Absorption curves of different l_2 under Ex polarization; (b) absorption curves of different l_2 under Ey polarization.

Figure 7 shows the influence of changing the upper side length l_3 of the trapezoid in the absorber structure on the absorption results when the other parameters remain unchanged. Figure 7a,b, respectively, show the changing absorption curves of the incident light with different l_2 lengths under Ex polarization and Ey polarization. In Figure 7a, it can be seen that the width of the absorption peak decreases gradually when l_3 decreases

from 0.6 μm , the width of the absorption peak exceeding the 80% absorption rate decreases from 1.7 μm to 1 μm when $l_3 = 0.2 \mu\text{m}$, and the absorption trough appears at 9 μm when l_3 increases from 0.6 μm to 1.0 μm . The absorption rate decreased to 70%, and the width of the absorption peak gradually increased. In Figure 7b, when the polarization angle is 90° , with the increase in l_3 length, the absorption at $\lambda = 12.3 \mu\text{m}$ has a slight increase. On the whole, the absorption effect of changing l_3 length has no obvious change.

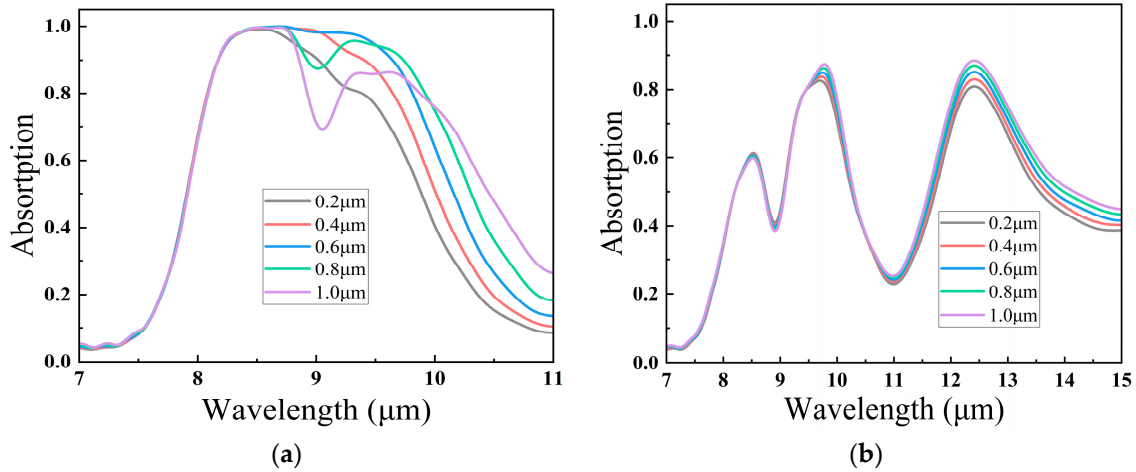


Figure 7. (a) Absorption curves of different l_3 under Ex polarization; (b) absorption curves of different l_3 under Ey polarization.

Figure 8 shows the influence of changing the height h_2 of the trapezoid in the absorber structure on the absorption results when the other parameter conditions are unchanged. Figure 8a,b, respectively show the changing absorption curves of the incident light with different h_2 lengths under Ex polarization and Ey polarization. It can be seen from Figure 8a that when the polarization angle of the incident light is 0° , the trapezoid height h_2 increases or decreases with the standard of 0.2 μm , and a gradually enhanced trough appears at 9 μm , and gradually redshifts with the increase of the height. When h_2 increases from 1.3 μm to 1.7 μm , the absorption rate decreases obviously, but it can be maintained at more than 85%. It can be seen from Figure 8b that when the polarization angle of incident light is 90° , the absorption rate in the far infrared band increases significantly with the increase of h_2 . When the height of h_2 decreases from 0.9 μm to 1.7 μm , the absorption rate at $\lambda = 12.3 \mu\text{m}$ increases from 80% to 90%.

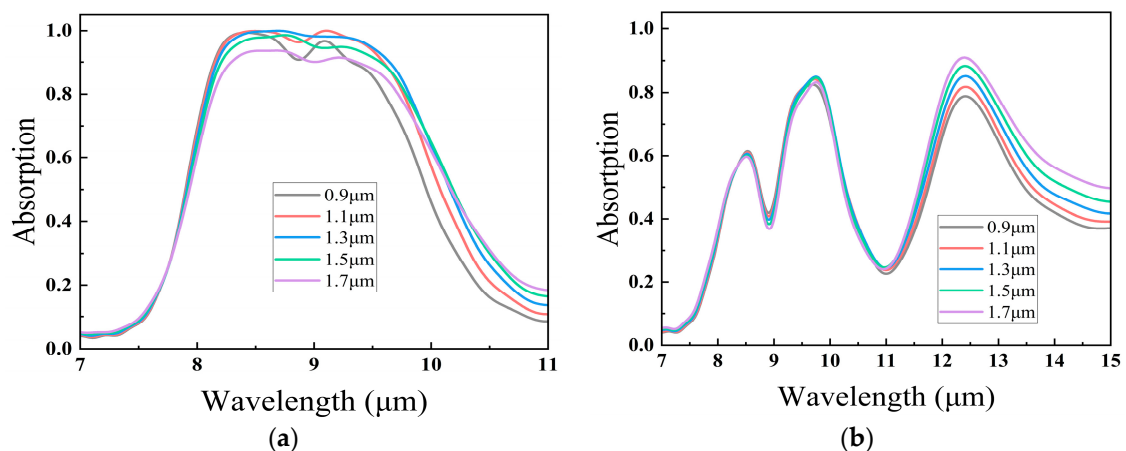


Figure 8. (a) Absorption curves of different h_2 under Ex polarization; (b) absorption curves of different h_2 under Ey polarization.

Figure 9 shows the influence of changing the height h_1 of the rectangle in the absorber structure on the absorption results under the condition of the other parameters unchanged. Figure 9a,b, respectively, show the changing absorption curves of the incident light with different h_1 lengths under Ex and Ey polarization. It can be seen from Figure 9a that when the polarization angle of incident light is 0° , the trapezoidal height h_1 increases or decreases with the standard of $2.5 \mu\text{m}$, and the absorption rate decreases. When h_1 increases from $2.5 \mu\text{m}$ to $2.9 \mu\text{m}$, a gradually deeper trough appears. It can be seen from Figure 9b that when the polarization angle of incident light is 0° , the absorption rate also increases significantly with the increase in h_1 .

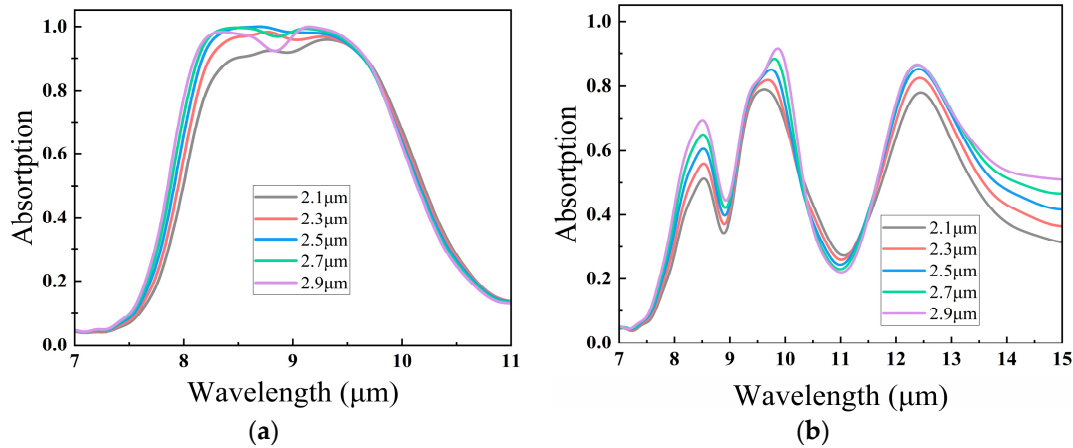


Figure 9. (a) Absorption curves of different h_1 under Ex polarization; (b) absorption curves of different h_1 under Ey polarization.

Figure 10 shows the influence of changing the side length l_4 of the rectangle in the absorber structure on the absorption results when the other parameter conditions are unchanged. Figure 10a,b, respectively, show the changing absorption curves of the incident light with different l_4 lengths under Ex polarization and Ey polarization. It can be seen from Figure 10a that when the rectangular side length l_4 gradually increased from $0.6 \mu\text{m}$ to $1.0 \mu\text{m}$, the absorption rate in the 8–9 μm band decreased significantly, while there was no significant change in the 9–11 μm band. It can be intuitively seen from Figure 10b that with the gradual increase in the length of l_4 , the absorption peak at $\lambda = 8.5 \mu\text{m}$ and $\lambda = 12.3 \mu\text{m}$ decreases, and the absorption peak at $\lambda = 9.7 \mu\text{m}$ increases.

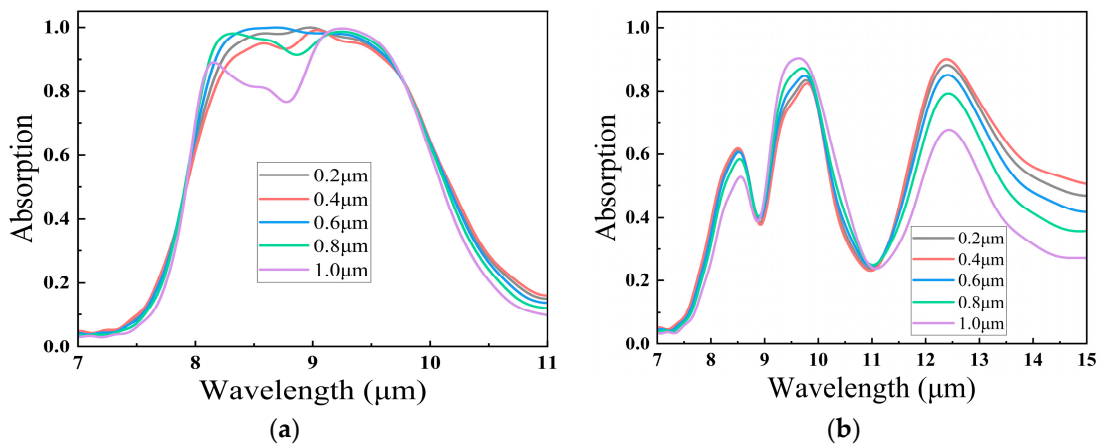


Figure 10. (a) Absorption curves of different l_4 under Ex polarization; (b) absorption curves of different l_4 under Ey polarization.

In the table, we summarize the sensitivity of each parameter when the incident light is Ex-polarized and Ey-polarized, and the results are shown in Table 1. When the polarization

angle of the incident light is 0° , we take the absorption width exceeding $1 \mu\text{m}$ when the absorption rate exceeds 80% as the tolerance error for statistical analysis. It can be obtained that the height h_2 of the trapezoid is a non-sensitive parameter. The height of the rectangle h_1 is a non-sensitive parameter, and the error requirements can be met within $2.8 \mu\text{m}$. Similarly, the lower side length l_2 of the trapezoid and the side length l_4 of the rectangle are both non-sensitive parameters. The upper side length l_3 of the trapezoid is a sensitive parameter, which can only achieve a width of more than $1 \mu\text{m}$ when the absorptivity exceeds 80% within the error range of $\pm 0.2 \mu\text{m}$. When the polarization angle of the incident light is 90° , the absorption rate of more than 80% at $\lambda = 12.3 \mu\text{m}$ is considered as an acceptable error. The height of the trapezoid h_2 , the height of the rectangle h_1 , the length of the upper side of the trapezoid l_3 , and the length of the lower side of the trapezoid l_2 are all non-sensitive parameters, and the length of the rectangle l_4 is a sensitive parameter, which can only meet the error requirements when the error is less than $0.6 \mu\text{m}$.

Table 1. Sensitivity statistics of various parameters of broadband absorber during Ex and Ey polarization.

	Parameters (μm)	Ex (Error μm)	Ey (Error μm)
The height of the trapezoid h_2	1.3	Non-sensitive parameters (≤ 2)	Non-sensitive parameters (-)
The height of the rectangle h_1	2.5	Non-sensitive parameters (≤ 2.8)	Non-sensitive parameters (-)
The upper side length of the trapezoid l_3	0.6	Sensitive parameters (± 0.2)	Non-sensitive parameters (-)
The lower side length of the trapezoid l_2	1	Non-sensitive parameters (0.6 to 1.4)	Non-sensitive parameters (≤ 1.4)
The width of the rectangle l_4	0.6	Non-sensitive parameters (≤ 1.0)	Sensitive parameters (≤ 0.6)

4. Conclusions

In this paper, a polarization selective broadband metamaterial absorber structure based on silica all-dielectric is proposed, which works in the long infrared band. The wide wavelength absorber is realized by combining different silica absorbers, and the broadband absorption in the long infrared band is realized. The calculated results show that the perfect absorption rate of the structure is more than 90% between $8.16 \mu\text{m}$ and $9.61 \mu\text{m}$. We calculated the absorption results of the metamaterial absorber at different polarization angles when the polarization angle of light increases from 0° to 90° ; that is, the light changes from Ex polarization to Ey polarization. When the polarization angle of the incident light is less than 45° , the absorption results of the absorber do not change significantly. When the polarization angle of the incident light is greater than 45° , three absorption peaks appear in the long infrared band, which realizes the selective characteristics of the incident light polarization. When the polarization angle is increased to 90° , the absorption rates of the two absorption peaks at $\lambda = 9.7 \mu\text{m}$ and $\lambda = 12.3 \mu\text{m}$ both reach more than 85%. Through the calculation and analysis of the changes of various parameters of the structure under Ex polarization and Ey polarization, it can be found that most of the parameters are not sensitive except for the upper side length of the trapezoid l_3 under Ex polarization, and except for the side length of the rectangle l_4 under Ey polarization. The tolerance error range is high, which is conducive to practical fabrication. These studies play a certain guiding role in the further development of non-metallic dielectric materials in metamaterial absorbers.

Author Contributions: Conceptualization, H.Z. (Haotian Zou) and B.N.; methodology, B.N.; software, H.Z. (Haotian Zou); validation, H.Z. (Haotian Zou) and B.N.; formal analysis, H.Z. (Haotian Zou), H.Z. (Hua Zhou) and J.C.; investigation, H.Z. (Hua Zhou) and B.N.; data curation, H.Z. (Haotian Zou); writing—original draft preparation, H.Z. (Haotian Zou); writing—review and editing, H.N. (Hua Zhou) and G.H. All authors have read and agreed to the published version of the manuscript.

Funding: This work was supported by the National Natural Science Foundation of China, Grant numbers 62175114 and 61875089, and the Kunshan and Nanjing University of Information Science and Technology (NUIST) intelligent sensor research center project.

Institutional Review Board Statement: Not applicable.

Informed Consent Statement: Not applicable.

Data Availability Statement: The data are available from the first author and the corresponding author upon reasonable request.

Conflicts of Interest: The authors declare no conflict of interest.

References

1. Shelby, R.A.; Smith, D.R.; Schultz, S. Experimental verification of a negative index of refraction. *Science* **2001**, *292*, 77–79. [[CrossRef](#)] [[PubMed](#)]
2. Chen, H.J.; Zhao, W.X.; Song, K. A “II-shaped” metamaterial with dual-band negative refraction index. *J. Northwest Norm. Univ.* **2018**, *54*, 49–53.
3. Leonhardt, U. Optical conformal mapping. *Science* **2006**, *312*, 1777–1780. [[CrossRef](#)] [[PubMed](#)]
4. Kim, J.; Seong, J.; Yang, Y.; Moon, S.W.; Badloe, T.; Rho, J. Tunable metasurfaces towards versatile metalenses and metaholograms: A review. *Adv. Photonics* **2022**, *4*, 024001. [[CrossRef](#)]
5. Ye, X.; Qian, X.; Chen, Y.X.; Yuan, R.; Xiao, X.; Chen, C.; Hu, W.; Huang, C.; Zhu, S.; Li, T. Chip-scale metalens microscope for wide-field and depth-of-field imaging. *Adv. Photonics* **2022**, *4*, 046006. [[CrossRef](#)]
6. Landy, N.I.; Sajuyigbe, S.; Mock, J.J.; Smith, D.R.; Padilla, W.J. Perfect metamaterial absorber. *Phys. Rev. Lett.* **2008**, *100*, 207402. [[CrossRef](#)]
7. Kong, H.; Li, G.; Jin, Z.; Ma, G.; Zhang, Z.; Zhang, C. Polarization-independent meta-material absorber for terahertz frequency. *J. Infrared Millim. Terahertz Waves* **2012**, *33*, 649–656. [[CrossRef](#)]
8. Grant, J.; Ma, Y.; Saha, S.; Khalid, A.; Cumming, D.R. Polarization insensitive, broadband terahertz metamaterial absorber. *Opt. Lett.* **2011**, *36*, 3476. [[CrossRef](#)]
9. Hao, J.; Yuan, Y.; Ran, L.; Jiang, T.; Kong, J.A.; Chan, C.T.; Zhou, L. Manipulating electromagnetic wave polarizations by anisotropic metamaterials. *Phys. Rev. Lett.* **2007**, *99*, 063908. [[CrossRef](#)]
10. Wang, H.; Prasad, S.V.; Mitchell, A.; Rosengarten, G.; Phelan, P.; Wang, L. Highly efficient selective metamaterial absorber for high-temperature solar thermal energy harvesting. *Sol. Energy Mater. Sol. Cells* **2015**, *137*, 235–242. [[CrossRef](#)]
11. Pendry, J.B. Negative refraction makes a perfect lens. *Phys. Rev. Lett.* **2000**, *85*, 3966–3969. [[CrossRef](#)] [[PubMed](#)]
12. Liu, S.; Chen, H.; Cui, T.J. A broadband terahertz absorber using multi-layer stacked bars. *Appl. Phys. Lett.* **2015**, *106*, 151601. [[CrossRef](#)]
13. Tao, H.; Bingham, C.; Pilon, D.; Fan, K.; Strikwerda, A.C.; Shrekenhamer, D.; Padilla, W.J.; Zhang, X.; Averitt, R.D. A dual band terahertz metamaterial absorber. *J. Phys. D Appl. Phys.* **2010**, *43*, 225102. [[CrossRef](#)]
14. Shen, X.; Cui, T.J.; Zhao, J.; Ma, H.F.; Jiang, W.X.; Li, H. Polarization-independent wide-angle triple-band metamaterial absorber. *Opt. Express* **2011**, *19*, 9401–9407. [[CrossRef](#)] [[PubMed](#)]
15. Wu, J. Tunable multi-band terahertz absorber based on graphene nano-ribbon metamaterial. *Phys. Lett. A* **2019**, *383*, 2589–2593. [[CrossRef](#)]
16. Nguyen, T.; Phan, H.L.; Tung, P.D.; Tuan, T.S.; Nguyen, H. Numerical Study of a Wide-Angle and Polarization-Insensitive Ultrabroadband Metamaterial Absorber in Visible and Near-Infrared Region. *IEEE Photonics J.* **2019**, *25*, 4600208.
17. Wu, S.; Li, J.S. Hollow-petal graphene metasurface for broadband tunable THz absorption. *Appl. Opt.* **2019**, *58*, 3023–3028. [[CrossRef](#)]
18. Li, D.; Huang, H.; Xia, H.; Zeng, J.; Li, H.; Xie, D. Temperature-dependent tunable terahertz metamaterial absorber for the application of light modulator. *Results Phys.* **2018**, *11*, 659–664. [[CrossRef](#)]
19. Kong, X.R.; Zhang, H.F.; Dao, R.N. A switchable polarization-independent THz absorber using a phase change material. *Opt. Quantum Electron.* **2019**, *51*, 306. [[CrossRef](#)]
20. Andrews, M.R.; Mitra, P.P.; Decarvalho, R. Tripling the capacity of wireless communications using electromagnetic polarization. *Nature* **2001**, *409*, 316–318. [[CrossRef](#)]
21. Mao, D.; Zheng, Y.; Zeng, C.; Lu, H.; Wang, C.; Zhang, H.; Zhang, W.; Mei, T.; Zhao, J. Generation of polarization and phase singular beams in fibers and fiber lasers. *Adv. Photonics* **2022**, *3*, 014002. [[CrossRef](#)]
22. Li, W.H.; Zhang, J.Q.; Qu, S.B.; Shen, Y.; Yu, J.; Fan, Y.; Zhang, A. A circular polarization antenna designed based on the polarization conversion metasurface. *Acta Phys. Sin.* **2016**, *65*, 024101.
23. Zhao, Y.X.; Qiu, C.; Wu, A.; Huang, H.; Li, J.; Sheng, Z.; Li, W.; Wang, X.; Gan, F. Broadband Polarization Splitter-Rotator and the Application in WDM Receiver. *IEEE Photonics J.* **2019**, *11*, 6600310. [[CrossRef](#)]
24. Xia, P.; Ri, S.E.; Inoue, T.; Awatsuji, Y.; Matoba, O. Dynamic phase measurement of a transparent object by parallel phase-shifting digital holography with dual polarization imaging cameras. *Opt. Lasers Eng.* **2021**, *141*, 106583. [[CrossRef](#)]

25. Zhang, Y.; Li, Y.; Cao, Y.; Liu, Y.; Zhang, H. Graphene induced tunable and polarization-insensitive broadband metamaterial absorber. *Opt. Commun.* **2017**, *382*, 281–287. [[CrossRef](#)]
26. Tao, H.; Bingham, C.; Strikwerda, A.C.; Pilon, D.; Shrekenhamer, D.; Landy, N.I.; Fan, K.; Zhang, X.; Padilla, W.; Averitt, R. Highly flexible wide angle of incidence terahertz metamaterial absorber design, fabrication, and characterization. *Phys. Rev. B Condens. Matter Mater. Phys.* **2008**, *78*, 241103. [[CrossRef](#)]
27. Li, Y.; An, B.; Li, L.; Gao, J. Broadband LWIR and MWIR absorber by trapezoid multilayered grating and SiO₂ hybrid structures. *Opt. Quantum Electron.* **2018**, *50*, 459. [[CrossRef](#)]
28. Long, L.; Yang, Y.; Liang, C. A wide-angle polarization-insensitive ultra-thin metamaterial absorber with three resonant modes. *J. Appl. Phys.* **2011**, *110*, 207402-R.
29. Zhou, R.L.; Kaleem, U.; Hussain, N.; Fadhali, M.M.; Yang, S.; Lin, Q.; Zubair, M.; Iqbal, M.F. Recent advances in photonics of three-dimensional Dirac semimetal Cd₃As₂. *Adv. Photonics* **2022**, *1*, 024001. [[CrossRef](#)]
30. Liu, H.F.; Luo, K.; Tang, S.H.; Peng, D.H.; Hu, F.J.; Tu, L.C. An Ultra-Wideband THz/IR Metamaterial Absorber Based on Doped Silicon. *Materials* **2018**, *11*, 2590. [[CrossRef](#)]
31. Yang, E.; Yang, F.L.; Pei, J.J.; Zhang, X.P.; Liu, S.M.; Deng, Y.Q. All-dielectric ultra-broadband metamaterial absorber based on imidazole ionic liquids. *J. Phys. D-Appl. Phys.* **2019**, *52*, 395501. [[CrossRef](#)]
32. Zhang, Y.; Dong, H.; Mou, N.; Li, H.; Yao, X.; Zhang, L. Tunable and transparent broadband metamaterial absorber with water-based substrate for optical window applications. *Nanoscale* **2021**, *13*, 7831–7837. [[CrossRef](#)]
33. Liu, F.; Zou, M.L.; Feng, Z.J.; Ni, B.; Ye, B.S.; Wang, Y.J. All-Dielectric Dual-Band Metamaterial Absorber Based on Ring Nanocavity in Visible Region for Sensing Applications. *Photonics* **2023**, *10*, 58. [[CrossRef](#)]
34. Si, J.; Liu, S.; Yang, W.; Yu, X.; Zhang, J.; Deng, X. Broadened Angle-Insensitive Near-Perfect Absorber Based on Mie Resonances in Amorphous Silicon Metasurface. *Nanomaterials* **2020**, *10*, 1733. [[CrossRef](#)]
35. Nils, O.L.; Ruggero, V.; Petter, J.; Mikael, K. Large-Scale Silicon Nanophotonic Metasurfaces with Polarization Independent Near-Perfect Absorption. *Nano Lett.* **2017**, *17*, 3054–3060.
36. Yang, S.C.; Richter, K.; Fischer, W.J. Multicolor generation using silicon nanodisk absorber. *Appl. Phys. Lett.* **2015**, *106*, 2649. [[CrossRef](#)]
37. Fang, B.; Li, B.; Peng, Y.; Li, C.; Hong, Z.; Jing, X. Polarization-independent multiband metamaterials absorber by fundamental cavity mode of multilayer microstructure. *Microw. Opt. Technol. Lett.* **2019**, *61*, 2385–2391. [[CrossRef](#)]
38. Chen, W.; Wang, S.; Jin, W.; Li, W. Research of infrared polarization characteristics based on polarization Micro-surface theory. *J. Infrared Millim. Waves* **2014**, *33*, 507–514.
39. Yang, Q.; Chen, X.; Xu, Q.; Tian, C.; Xu, Y.; Cong, L.; Zhang, X.; Li, Y.; Zhang, C.; Zhang, X.; et al. Broadband terahertz rotator with an all-dielectric metasurface. *Photonics Res.* **2018**, *6*, 1056–1061. [[CrossRef](#)]
40. Palik, E.D. *Handbook of Optical Constants of Solids II*; Academic Press: Boston, MA, USA, 1991; Volume 1, pp. 77–135.

Disclaimer/Publisher's Note: The statements, opinions and data contained in all publications are solely those of the individual author(s) and contributor(s) and not of MDPI and/or the editor(s). MDPI and/or the editor(s) disclaim responsibility for any injury to people or property resulting from any ideas, methods, instructions or products referred to in the content.